




RESEARCH ARTICLE | SEPTEMBER 18 2024

The “simple” photochemistry of thiophene

Michael A. Parkes ; Graham A. Worth  



J. Chem. Phys. 161, 114305 (2024)

<https://doi.org/10.1063/5.0226105>



Articles You May Be Interested In

Photochemistry of Biological Chemosensors, Organic Light-Emitting Diodes, and Inner-shell Electronic Processes

AIP Conference Proceedings (April 2008)

A resonance Raman spectroscopic and CASSCF investigation of the Franck–Condon region structural dynamics and conical intersections of thiophene

J. Chem. Phys. (October 2010)

Role of surface crossings in the photochemistry of nitromethane

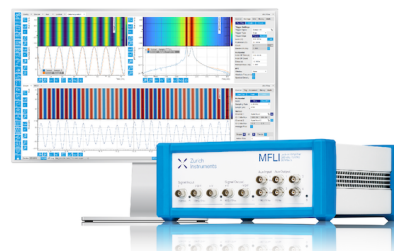
J. Chem. Phys. (February 2005)

Challenge us.

What are your needs for periodic signal detection?



[Find out more](#)



The “simple” photochemistry of thiophene

Cite as: J. Chem. Phys. 161, 114305 (2024); doi: 10.1063/5.0226105

Submitted: 29 June 2024 • Accepted: 2 September 2024 •

Published Online: 18 September 2024



View Online



Export Citation



CrossMark

Michael A. Parkes^{a)}  and Graham A. Worth^{b)} 

AFFILIATIONS

Department of Chemistry, University College London, 20 Gordon St., London WC1H 0AJ, United Kingdom

^{a)}michael.parkes@ucl.ac.uk

^{b)}Author to whom correspondence should be addressed: g.a.worth@ucl.ac.uk

ABSTRACT

The static gas-phase (“simple”) ultraviolet absorption spectrum of thiophene is investigated using a combination of a vibronic coupling model Hamiltonian with multi-configuration time-dependent Hartree quantum dynamics simulations. The model includes five states and all 21 vibrations, with potential surfaces calculated at the complete active space with second-order perturbation level of theory. The model includes terms up to eighth-order to describe the diabatic potentials. The resulting spectrum is in excellent agreement with the experimentally measured spectrum of Holland *et al.* [Phys. Chem. Chem. Phys. **16**, 21629 (2014)]. The, until now not understood, spectral features are assigned, with a combination of strongly coupled vibrations and vibronic coupling between the states giving rise to a progression of triplets on the rising edge of the broad spectrum. The analysis of the underlying dynamics indicates that population transfer between all states takes place on a sub-100 fs timescale, with ring-opening occurring at longer times. The model thus provides a starting point for further investigations into the complicated photo-excited dynamics of this key hetero-aromatic molecule.

© 2024 Author(s). All article content, except where otherwise noted, is licensed under a Creative Commons Attribution (CC BY) license (<https://creativecommons.org/licenses/by/4.0/>). <https://doi.org/10.1063/5.0226105>

I. INTRODUCTION

Thiophene is the prototypical sulfur containing heterocycle, with a similar structure to furan but with the O atom replaced with an S atom (see the inset of Fig. 1). Thiophene has come to play a central role in advances in optoelectronics as it is the basis of a wide range of polymers and oligomers that find use as photovoltaics, molecular switches, and even light emitting diodes.¹ It is the intrinsic properties of thiophene and thiophene containing polymers, such as efficient light harvesting and charge transfer, that make them such a popular choice. It is therefore surprising that thiophene’s gas-phase photochemistry is actually not well understood.

A range of theoretical and experimental studies have been performed on thiophene focusing on its first excitation band, which lies in the UV and is shown in Fig. 1. This band is quite broad but possesses a well resolved set of vibrational progressions on the rising edge. Recently, two high-resolution VUV absorption studies have been published.^{2,3} These studies concluded that the first band is made up of two closely spaced valence states: $^1A_1(\pi_2 - \pi_1^*)$ and $^1B_2(\pi_1 - \pi_1^*)$. The precise ordering of these states and their energies are hard to determine and are highly dependent on the type of *ab initio* calculation and basis set used.^{2,4,5} Furthermore, the vibrational progression defies a clear assignment. There is some

agreement that the band origin is the peak at 5.16 eV and that the vibrational structure below that is due to hot bands.⁶ However, the spacing of the progressions does not match that of any known vibrational modes of thiophene, although a tentative assignment has been made to ν_6 . In addition, the spacing within each progression is much smaller than the frequency of any of the modes of thiophene, indicating that there is a strong vibronic coupling between the two electronic states.^{2,7}

Three experiments have looked at thiophene’s excited state dynamics: one in an indirect manner and the other two directly. Wu *et al.* used resonance Raman spectroscopy to look indirectly at the vibronic coupling of thiophene in cyclohexane.⁸ They observed that five symmetric A_1 modes and three antisymmetric (two B_2 and one A_2) modes were important when thiophene was excited into S_1 . Their experiments suggest that dynamics in the Franck–Condon region are along the in-plane C–S and C–C ring stretches, with ring opening occurring by crossing into a B_2 electronic state; they also expect crossing into an A_2 state.

Direct experimental measurements have used UV femtosecond pump–probe spectroscopy to examine the gas-phase dynamics of thiophene.^{9,10} Weinkauff *et al.* used a 238 nm pump to excite to S_1 with a 276 nm probe.⁹ By combining their experimental results with a simulation, they extracted two time constants, a fast decay on the

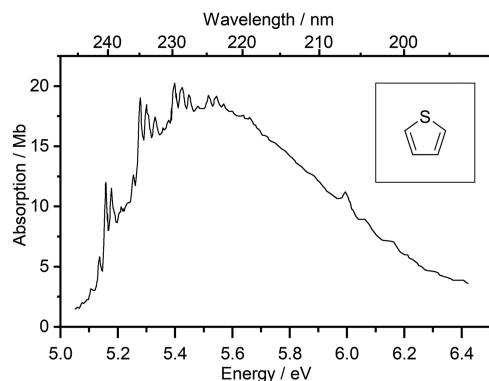


FIG. 1. UV-Vis spectrum of the first band of thiophene, taken from Holland *et al.* with permission of the publisher.² The structure of thiophene is shown in the inset.

S_1 potential energy surface from the S_0 geometry (Franck–Condon point) to the S_1 minimum (80 fs). This decay was then followed by an ultrafast (25 fs) decay from S_1 to “S3,” a state that corresponds to S_3 at the Franck–Condon point. This leads to opening of the thiophene ring. In addition, they observed a long-lived component that did not decay in the time-frame of their experiment (>50 ps); this was attributed to ionization of the now linear form of thiophene. Schalk *et al.* used a 200 nm pump to excite to S_2 , and with a 280 nm probe, they extracted similar decays to Weinkauff *et al.*, plus a 450 fs delay that Weinkauff did not observe.¹⁰ They concluded that the faster decays are ring puckering motions, while the slow decay might indicate a ring opening process. We note that in both experiments, the experimental cross correlation was >160 fs, making extraction of ultrafast decays difficult.

Due to these experimental difficulties in understanding the dynamics, following photoexcitation several groups have attempted to use theory to gain insights using different theoretical methods, including time-dependent (TD)-density functional theory (DFT), multi-reference configuration interaction DFT (DFT-MRCI), complete active space with second-order perturbation (CASPT2), and surface hopping methods.^{4,7,11–15} From these, some broad conclusions have been reached: first, the ordering of the first two excited states: S_1 has A_1 symmetry, while S_2 has B_2 symmetry. The ordering of the higher lying states has not been agreed on and again varies with theory and basis set used. From both simulations and calculation of stationary points, it seems that following photoexcitation, thiophene can undergo both ring-opening and ring-puckering motions. Although the relative contributions and timescales of these motions are still not agreed upon the consensus is that ring opening will be dominant. There is, however, disagreement on whether the triplet states of thiophene are involved or not. Prlj *et al.* performed surface hopping calculations with ADC(2) surfaces and were able to model the broad features of thiophene’s first excitation band (although the vibrational progression was not present) and found no contribution from crossing to the triplet states.⁴ In contrast, Schnappinger *et al.* used the Surface Hopping with Arbitrary Couplings (SHARC) surface hopping method with complete active space self-consistent field (CASSCF) surfaces and found that triplet states do play a role.¹²

Two previous studies have applied a linear vibronic coupling (LVC) model Hamiltonian to thiophene. Köppel *et al.* used an

LVC model and the Multiconfiguration Time-Dependent Hartree (MCTDH) method to look at the spectroscopy of furan, pyrrole, and thiophene.⁷ Though obtaining good agreement with experiment for furan and pyrrole, for thiophene the extensive vibrational structure was not captured correctly. In the second study, the experimental work of Holland *et al.* was supported by use of an LVC model to determine the position of the adiabatic excitation energies of the electronic states.² As noted in this work, a proper understanding of the absorption structure of thiophene requires additional calculations, which include vibronic coupling and nuclear dynamics.

Given thiophene’s importance for organo-electronics, it is essential to make sure we understand the fundamental molecular properties of isolated thiophene. We have therefore applied the vibronic coupling model to construct a model Hamiltonian, but going to higher orders of expansion than used previously. MCTDH was then used to solve the time-dependent Schrödinger equation and obtain the absorption spectrum and population dynamic with an aim to understand the source of the vibrational progression and what dynamical processes are occurring following the photoexcitation of thiophene.

II. METHODOLOGY

A. The vibronic coupling model Hamiltonian

The vibronic coupling (VC) model uses diabatic potential energy surfaces (PESs) generated from *ab initio* adiabatic surfaces. The use of a diabatic potential removes singularities at points where two PESs meet at a conical intersection. These diabatic surfaces are generated by assuming that the PESs are smooth and that the diabatic potential matrix (\mathbf{W}) can be defined as Taylor expansions around a reference point (usually the Franck–Condon region, but any convenient point can be used). This generates the following model Hamiltonian:

$$\mathbf{H} = \mathbf{H}^{(0)} + \mathbf{W}^{(0)} + \mathbf{W}^{(1)} + \mathbf{W}^{(2)} + \dots \quad (1)$$

The zeroth order matrices ($\mathbf{H}^{(0)}$ and $\mathbf{W}^{(0)}$) are diagonal and defined in the following manner:

$$H_{ij}^{(0)}(Q) = \sum_{\alpha} \left(-\frac{\omega_{\alpha}}{2} \frac{\partial^2}{\partial Q_{\alpha}^2} + \frac{\omega_{\alpha}}{2} Q_{\alpha}^2 \right) \delta_{ij}, \quad (2)$$

$$W_{ij}^{(0)}(Q) = E_i \delta_{ij}, \quad (3)$$

where ω_{α} are the frequencies of vibrational mode α , Q_{α} are the mass–frequency scaled normal mode coordinates, and E_i are the energies of the electronic state at the point where the Taylor expansion is evaluated. At this point, the diabatic and adiabatic states are the same by definition.

In what is commonly referred to as the Quadratic Vibronic Coupling (QVC) model, the remaining terms in the diabatic expansion are then given by the following expressions:

$$W_{ii}^{(1)}(Q) = \sum_{\alpha} \kappa_{\alpha}^{(i)} Q_{\alpha}, \quad (4)$$

$$W_{ij}^{(1)}(Q) = \sum_{\alpha} \lambda_{\alpha}^{(i,j)} Q_{\alpha}, \quad (5)$$

$$W_{ii}^{(2)}(Q) = \sum_{\alpha,\beta} \frac{1}{2} \gamma_{\alpha,\beta}^{(i)} Q_{\alpha} Q_{\beta}. \quad (6)$$

The on-diagonal linear terms affect the vibrational modes within an electronic state, and the coefficients, $\kappa_{\alpha}^{(i)}$, represent the gradients of the *ab initio* surfaces at the Franck–Condon point. Due to symmetry restrictions, only the A_1 vibrational modes of thiophene can have a non-zero κ value.

The off-diagonal linear coupling terms with coefficients $\lambda_{\alpha}^{(ij)}$ couple the different electronic states i and j , and hence, vibrations α with a non-zero λ parameter are termed coupling modes. As with the κ parameters, symmetry limits which states are coupled by which vibrations. Pairs of states will only have a non-zero λ parameter if the product of the vibrational and state symmetries contains the totally symmetric representation. For example, in the C_{2v} point group that thiophene belongs to, the states S_1 and S_2 of A_1 and B_2 symmetries, respectively, are coupled by modes with the B_2 symmetry.

The higher-order quadratic terms ($\gamma_{\alpha\beta}^{(i)} Q_{\alpha} Q_{\beta}$) represent the frequency shifts of the excited state relative to the ground state and also Duschinsky rotations where the normal modes are mixed within a state. This model describes the potential surfaces and vibronic coupling based around the Franck–Condon point and assuming that the diabatic potentials are harmonic. In thiophene, however, the strong anharmonicity of the potential surfaces and strong coupling between the vibrational modes mean that it is necessary to go to higher orders in the Taylor expansions defining the diabatic potentials, W_{ii} , and couplings, W_{ij} , as explained in Sec. III A. The symmetry rules for non-zero parameters are simple extensions of those described for the linear terms above. Similar high-order expansions to the vibronic coupling model have been used in earlier studies on cations and Jahn–Teller systems.^{16–18}

B. *Ab initio* calculations

To generate the diabatic surfaces, the adiabatic singlet surfaces of thiophene were calculated at the CASPT2 level using Molpro 2015¹⁹ with the 6-31G* basis set. The complete active space (CAS) of Schnappinger *et al.* was used.¹² This consists of a ten electron nine orbital active space. The orbitals in the active space included all the π -orbitals and the C–S σ -orbitals. Previous work has shown that the C–S σ -orbitals must be included for a correct description of the dynamics on the excited state surfaces.¹² See Fig. 2 for the orbitals included in the active space.

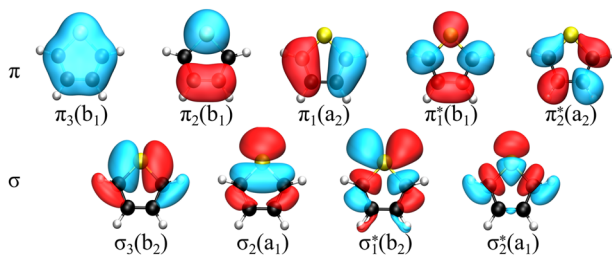


FIG. 2. Molecular orbitals included in the active space.

All calculations used a state-averaged CAS over the lowest five singlet states (ground-state plus four excited-states) and are thus designated SA5-CAS(10,9). Test calculations were performed including a sixth excited state, but this sixth state was found to be too high in energy to be important. The ground state structure of thiophene was optimized at the SA5-CAS(10,9) level. From the optimized structure, the vibrational frequencies of all 21 modes of thiophene were calculated, also at the SA5-CAS level. Excited-state calculations used CASPT2 (RS2C) on top of the SA5-CAS.

The parameters for the LVC model in Sec. II A are related to the potential gradients, Hessians, and derivative coupling vectors at the Franck–Condon point, $\mathbf{Q}_0 = 0$,

$$\kappa_{\alpha}^{(i)} = \left. \frac{\partial V^{(i)}}{\partial Q_{\alpha}} \right|_{\mathbf{Q}_0}, \quad (7)$$

$$\gamma_{\alpha\beta}^{(i)} = \left. \frac{\partial^2 V^{(i)}}{\partial Q_{\alpha} \partial Q_{\beta}} \right|_{\mathbf{Q}_0}, \quad (8)$$

$$\lambda_{\alpha}^{(i,j)} = F_{\alpha}^{(i,j)}(\mathbf{Q}_0), \quad (9)$$

where V^i is the adiabatic potential of state i and $F_{\alpha}^{(i,j)}$ is the non-adiabatic coupling vector between states i and j . These quantities can thus be obtained from quantum chemistry calculations. This was done using the quantum chemistry method described above to provide the LVC model Hamiltonian.

To obtain these high-order expansion parameters, cuts through the CASPT2 potential surface were calculated at points along every normal mode and, where necessary, points along diagonal cuts between two modes. These cuts provide adiabatic surfaces for the vibronic coupling model. Diabatic curves were then constructed that, upon diagonalization, provide a good fit to the adiabatic energies. This fitting was performed using the Vibronic Coupling HAMiltonian (VCHAM) programs²⁰ in the Quantics suite.^{21,22} The LVC model parameters derived from Eqs. (7)–(9) were used to provide initial guess values for the κ , λ , and γ coefficients in the fitting.

C. Quantum dynamics simulations

The Multiconfiguration Time-Dependent Hartree (MCTDH) method is a well-established way to solve the time-dependent Schrödinger equation for molecular systems.²³ The method has been extensively reviewed,^{24–26} so only the main points will be covered here. For a given Hamiltonian, here, the VC model of thiophene, the time-dependent Schrödinger equation, is solved by propagating the wavefunction. The MCTDH wavefunction is expanded in the following way:

$$\psi(\mathbf{Q}, t) = \sum_{j_1=1}^{n_1} \dots \sum_{j_p=1}^{n_p} \sum_{s=1}^{n_s} (t) \prod_{\kappa=1}^p \varphi_{j_{\kappa}}^{(\kappa)}(q_{\kappa}, t) |s\rangle. \quad (10)$$

Here, $A_{j_1 \dots j_p}$ are the time-dependent expansion coefficients and $\varphi_{j_{\kappa}}^{(\kappa)}$ are the time-dependent basis functions, known as single particle functions (SPFs), for coordinates q_{κ} . The coordinates are groups of physical coordinates, $q_{\kappa} = (Q_1, Q_2, \dots)$, to reduce the

number of sets of functions required and hence keep the expansion compact. The SPFs are represented by time-independent primitive basis functions: in this work, all the modes of thiophene used harmonic oscillator discrete variable representations.²⁴ The vector $|s\rangle$ represents the electronic states of the system. The time-evolution of the expansion coefficients and SPFs are then found using variational equations of motion. The combination of MCTDH and vibronic coupling Hamiltonians has been highly successful in modeling the short-time response of a range of photo-excited molecules.²⁵ Recent examples are maleimide²⁷ and cyclobutadiene.¹⁷

The computational effort, however, scales exponentially with the number of particles, p , as well as the size of the multi-dimensional grids describing the SPFs. For large systems, the effort can be reduced by using the multi-layer MCTDH (ML-MCTDH) variant.^{28–30} In this, the multi-mode SPFs are not directly expanded on a grid, but expanded using the MCTDH form using lower-dimensional SPFs in a second layer. These SPFs can be further expanded in lower layers, with the final layer expanded on primitive basis grids. The structure of the ML-MCTDH wavefunction can be described by a tree graph.²⁹ The one used for the calculations here is shown in Fig. S3 of the [supplementary material](#). The key for efficiency is constructing a tree in which strongly coupled modes are close together.

The photo-absorption spectrum of thiophene was simulated by taking the Fourier transform of the autocorrelation function of the ML-MCTDH wavefunction,

$$I(\omega) \sim 2 \operatorname{Re} \int_0^T e^{i\omega t} C(t) dt, \quad (11)$$

$$C(t) = \langle \psi^* (\frac{t}{2}) | \psi (\frac{t}{2}) \rangle, \quad (12)$$

where the use of the wavefunction at $\frac{t}{2}$ is valid for real initial wavefunctions²⁴ and allows an autocorrelation function to be obtained for twice the length of the propagation. Corrections are applied to this transform to allow for the finite propagation time of the simulation. For this, a cosine function is applied to make sure that the autocorrelation function becomes zero at the total propagation time, T . The correction also includes an exponential damping term $[\exp(-t/\tau)]$, which allows for the finite experimental resolution. $\tau = 150$ fs was used in the following.

Calculations were converged with respect to the spectrum and diabatic state populations. The latter are obtained directly from the wavefunction coefficients related to each state. Convergence is ensured by increasing the basis set until the results do not change. This was done by selecting a maximum basis set size (shown in Fig. S3) and increasing the number of SPFs for each node dynamically,³¹ making use of the natural orbital populations related to a set of SPFs by the associated reduced density matrix,

$$\rho_{ij}^{(\kappa)} = \sum_j' A_{j_i}^* A_{j_j}^{\kappa}, \quad (13)$$

where $A_{j_i}^{\kappa}$ is an expansion coefficient with the index i for mode κ and the sum is over all coefficients, except for those of the mode of interest, denoted by the prime on the summation. This is written for a single layer MCTDH form, but the form is equivalent for any node in a ML-MCTDH wavefunction. The eigenvalues

of this density matrix are the natural populations and provide a measure of importance for the SPFs in describing the wavefunction: low natural populations indicate that the space spanned by the SPFs is a good basis set. In the dynamical SPF procedure, SPFs are added to keep the population of the least populated natural orbitals below a given threshold.

D. Note on labeling electronic states

In the following, the electronic states in the adiabatic picture are labeled according to their state ordering and symmetry, i.e., $S_0(A_1)$, $S_1(A_1)$, $S_2(B_2)$, $S_3(B_1)$, and $S_4(A_2)$. In the diabatic picture, the states are labeled \tilde{X} , \tilde{A} , \tilde{B} , \tilde{C} , and \tilde{D} , and these correlate with the ordered adiabatic states at the Franck–Condon point, i.e., where the molecular coordinates are those of the ground-state equilibrium geometry $\tilde{X} = S_0$, $\tilde{A} = S_1$, $\tilde{B} = S_2$, $\tilde{C} = S_3$, and $\tilde{D} = S_4$.

III. RESULTS AND DISCUSSION

A. Vibronic coupling model

The energies and symmetries of the five lowest states of thiophene at the CASPT2 level are given in [Table I](#). It should be noted that calculations at the CAS level with this active space produce a different ordering of the states. The four excited states are found to be very close in energy, spanning 0.6 eV. The S_1 and S_2 states are both bright at the Franck–Condon point. The calculated normal modes and vibrational frequencies are listed in [Table II](#) and compared to the experimental values. The images of the vibrations are given in the [supplementary material](#).

The normal modes associated with the frequencies in [Table II](#) form the basis for the vibronic coupling Hamiltonian after transforming to mass–frequency scaled normal modes. Energies for all five states at the CASPT2 level of theory were calculated at points along all 21 coordinates as well as diagonal cuts between the key modes, and the VC model Hamiltonian parameters optimized to fit these energies. The key coupling constants of the VC model are given in [Tables S2 and S3](#) in the [supplementary material](#). The full set of parameters is also provided as a Quantics operator file in the provided datasets. Only the strongest coupling parameters are listed

TABLE I. Calculated properties of the first five electronic states of thiophene from a CASPT2 calculation with a 6-31G* basis set. The symmetries of the states, the energies (with oscillator strengths in parentheses), and the main transition are given. Experimental values are vertical transition energies taken from [Ref. 2](#).

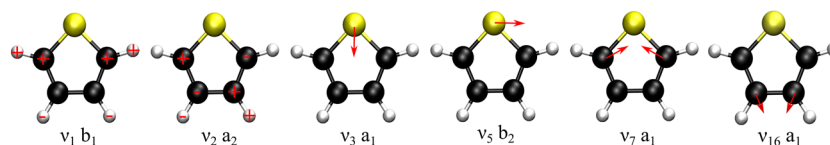
State	Symmetry	CASPT2 (eV) (f)	Transition	Experimental energies (eV)
S_0	A_1	0	...	0
S_1	A_1	5.641 (0.59)	$\pi_2 \rightarrow \pi_1^*$ ($b_1 \rightarrow b_1$)	5.64
S_2	B_2	6.070 (0.71)	$\pi_1 \rightarrow \pi_1^*$ ($a_2 \rightarrow b_1$)	5.97
S_3	B_1	6.203 (0.05)	$\pi_1 \rightarrow \sigma_1^*$ ($a_2 \rightarrow b_2$)	6.17
S_4	A_2	6.249 (0.00)	$\pi_2 \rightarrow \sigma_1^*$ ($b_1 \rightarrow b_2$)	6.33

TABLE II. Calculated and experimental vibrational modes of thiophene. Experimental data are taken from the NIST Chemistry WebBook.³² For the vibrational character, the main type of vibrational motion is indicated with the atoms involved and whether the vibration is ip = in-plane, op = out-of-plane, sym = symmetric, or asym = anti-symmetric.

Mode number and symmetry	Calculated frequency (eV) (cm ⁻¹)	Experimental frequency (cm ⁻¹)	Character
1 b ₁	0.055 444.40	452	Ring op
2 a ₂	0.071 572.38	567	Ring op
3 a ₁	0.074 602.46	608	C–S–C ip
4 a ₂	0.087 709.28	688	C–H op
5 b ₂	0.090 730.38	751	S ip
6 b ₁	0.091 736.74	712	C–H op
7 a ₁	0.101 816.61	839	C–S–C ip
8 b ₂	0.113 911.50	872	C ip
9 b ₁	0.113 911.67	867	C–H op
10 a ₂	0.116 938.83	903	C–H op
11 a ₁	0.136 1100.39	1036	C–H ip
12 b ₂	0.148 1193.83	1085	C–H ip
13 a ₁	0.148 1194.61	1083	C–H ip
14 b ₂	0.173 1398.60	1256	C–H ip
15 a ₁	0.186 1504.98	1360	C ip
16 a ₁	0.193 1558.35	1409	C ip
17 b ₂	0.207 1676.14	1504	C ip
18 b ₂	0.420 3387.27	3086	asym C–H
19 a ₁	0.421 3402.02	3098	sym C–H
20 b ₂	0.426 3435.98	3125	asym C–H
21 a ₁	0.426 3437.96	3126	sym C–H

in the tables, defined by $\kappa_{\alpha}^{(i)}/\omega_{\alpha} > 0.2$ or $\lambda_{\alpha}^{(ij)}/\omega_{\alpha} > 0.2$. These coupling strengths relate to the shift of a harmonic oscillator minimum from the Franck–Condon point due to the gradient at that point and thus relate to the level of excitation a mode receives on excitation.

Only the totally symmetric vibrations can have non-zero values of κ , and, as shown in Table S2, all these modes except for the high frequency modes ν_{19} and ν_{21} have significant values. This shows that for all states, the gradients of the potential surfaces at the Franck–Condon point are non-negligible and the excited-state minima for all states are significantly displaced from the ground-state equilibrium geometry. The coupling, λ , parameters in Table S3 show that there are a large number of significant couplings between the states. In fact, all vibrations except for the highest four frequencies are involved.

**FIG. 3.** Key normal modes ν_1 , ν_2 , ν_3 , ν_5 , ν_7 , and ν_{16} .

To provide a good fit of the adiabatic surfaces for the five states of thiophene, the high-order expansion terms listed in Table S4 of the [supplementary material](#) were added to the simple LVC model. These were chosen according to the shapes of the potentials and the symmetry of the modes involved, i.e., the product of the symmetries of the modes and states involved in a term has to be totally symmetric. The diabatic potentials along most modes for most states include a fourth order parameter to account for symmetric anharmonicity away from the Franck–Condon point, with modes 3 and 7 requiring a sixth order term to keep them bound. The modes with the A₁ symmetry can also take a third-order parameter to increase the asymmetry of the potentials.

These additional terms thus retain the symmetry of the Hamiltonian, which has been shown to be important for good results in studies on high symmetry Jahn–Teller systems.^{16,33} They are also complete up to fourth-order in the set of key, highly anharmonic modes, and the final surfaces are thus adequate for describing the short term dynamics of the thiophene system. More details on how the terms were selected are given in the [supplementary material](#).

The final model has a total of 707 parameters. For the final Hamiltonian, 2967 points were included in the fit. The overall root mean square deviation (RMSD) of the energies at the points from the quantum chemistry and the model is 0.39 eV. This drops to 0.21 eV if only points with energies below 8 eV are considered. This is not an insignificant error, but the restricted form of the potentials means that some regions, mostly away from the Franck–Condon point, are not well fitted. By inspection, the key regions around the Franck–Condon point look to be well described.

From the optimized parameters, in most states high-order terms provide coupling between modes ν_1 , ν_2 , and ν_3 . Modes ν_3 , ν_5 , and ν_7 are also strongly coupled. The key vibrations are thus ν_1 , ν_2 , ν_3 , ν_5 , and ν_7 , and these vibrations are shown in [Fig. 3](#). The cuts through the fitted potential energy surfaces along these key modes are shown in [Fig. 4](#) with cuts along the pairs of modes in [Fig. 5](#). The cuts along the remaining modes are shown in the [supplementary material](#).

The totally symmetric vibrations ν_3 and ν_7 are responsible for the symmetric sulfur motion and ring compression, respectively. The cuts along these modes in [Figs. 4\(c\)](#) and [4\(e\)](#) show the close nature of the four excited states. The cut along ν_3 is particularly dramatic, with the \tilde{C} and \tilde{D} diabatic potentials falling sharply to end up below the \tilde{A} and \tilde{B} states at negative displacements, with a double well on the adiabatic S₁ state resulting. While it is not found to be important for the description of the spectrum, and it does not couple strongly to the other modes, the cut along the totally symmetric mode ν_{16} is also shown in [Fig. 4\(f\)](#). It is a ring stretch, and there is a low lying crossing between S₁ and S₂ (diabatic states \tilde{A} and \tilde{B}) to positive displacement.

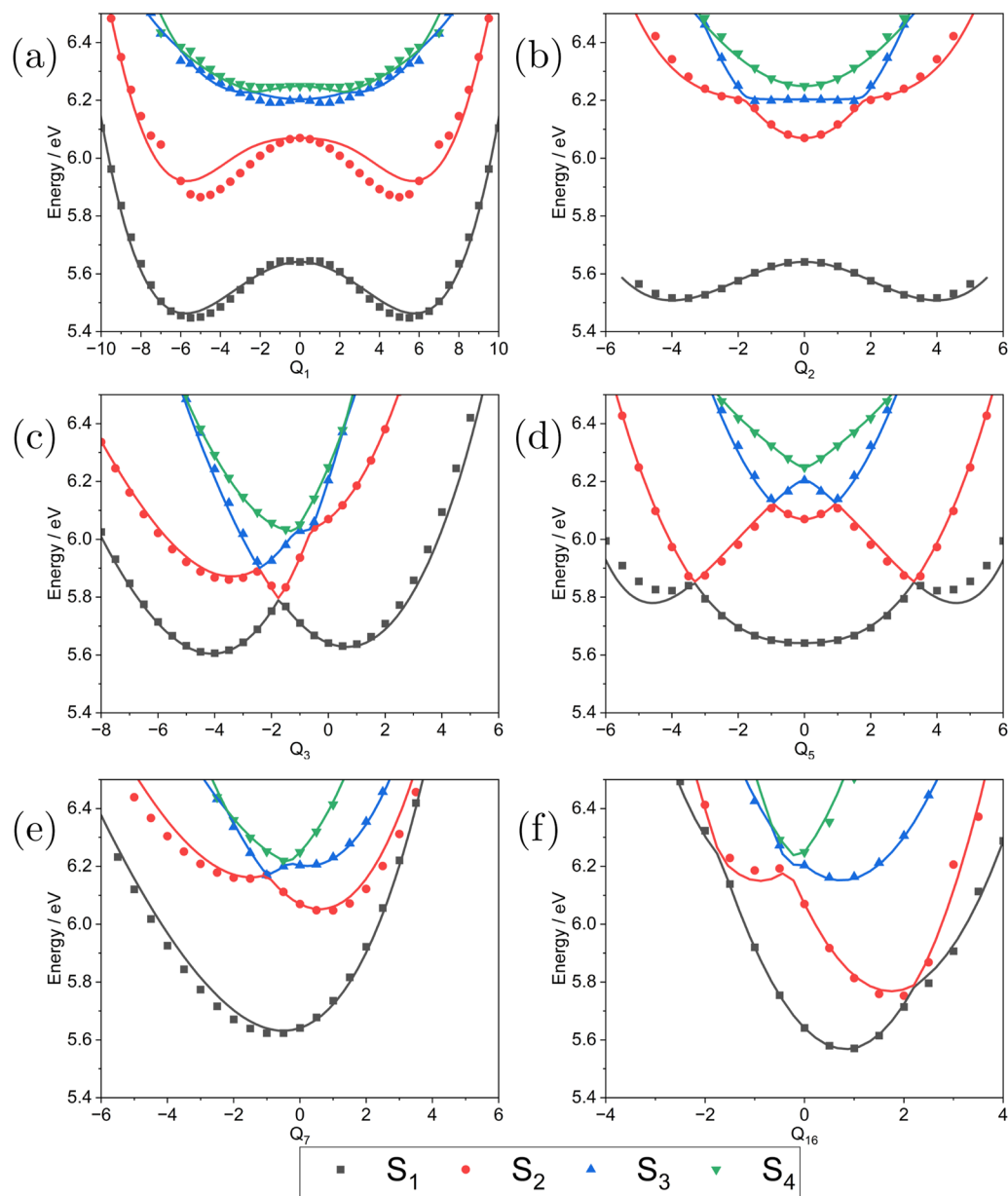


FIG. 4. Cuts along the selected mass-weighted normal modes for thiophene. (a) Q_1 , (b) Q_2 , (c) Q_3 , (d) Q_5 , (e) Q_7 , and (f) Q_{16} . Only states S_1 to S_4 are shown.

The b_2 mode ν_5 represents the asymmetric sulfur motion across the ring. The cuts along this mode in Fig. 4(d) also show a large deviation from the harmonic behavior of states \tilde{C} and \tilde{D} , with the \tilde{C} state again dropping rapidly in energy and ending up below the \tilde{A} state at large displacements and forming minima on the adiabatic S_1 . Modes ν_1 and ν_2 with b_1 and a_2 symmetries, respectively, are out-of-plane carbon motions. They both form double well potentials for all the excited states [Figs. 4(a) and 4(b)], but an energy gap is retained between S_1 and the higher excited states.

The cuts through the potential surfaces along the diagonal between modes are shown in Fig. 5. High-order terms coupling the vibrations are required to describe these strongly anharmonic regions of the surfaces. The cut Q_{3-5} between ν_3 and ν_5 [Fig. 5(d)] is particularly dramatic, with the S_1 minimum to a large negative displacement dropping over 0.5 eV below the curves seen along the cuts in Figs. 4(c) and 4(d). The mixing of ν_3 with the non-symmetric ν_1 and ν_2 vibrations [Figs. 5(b) and 5(c)] provides a complicated structure to the potential crossings that is hard to fit. The potential

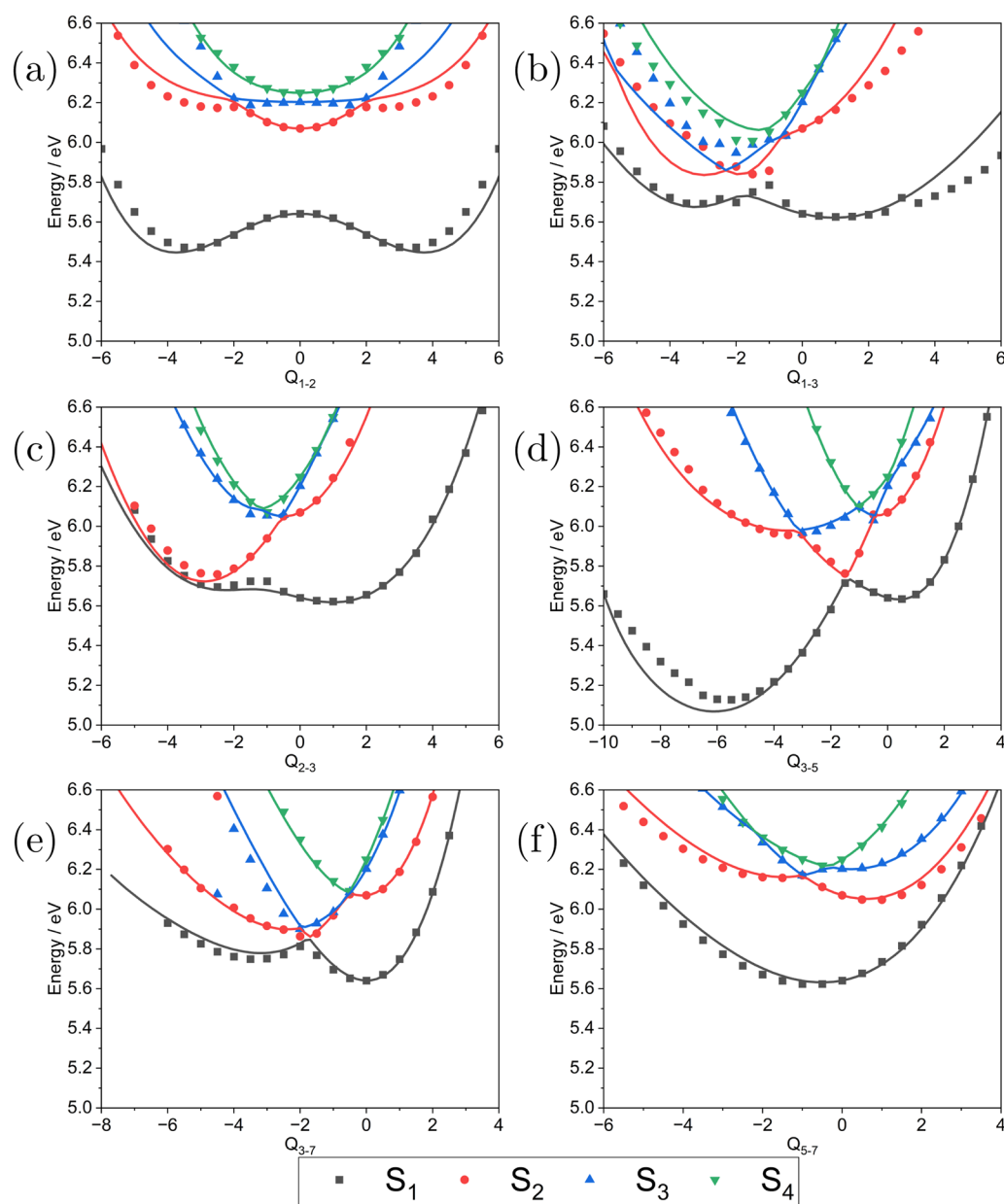


FIG. 5. Cuts through the potential energy surfaces diagonally between pairs of mass–frequency scaled normal modes for thiophene. All other coordinates are at the equilibrium geometry values. Cuts shown are between the following pairs of modes (a) Q_1/Q_2 , (b) Q_1/Q_3 , (c) Q_2/Q_3 , (d) Q_3/Q_5 , (e) Q_3/Q_7 , and (f) Q_5/Q_7 . Only states S_1 to S_4 are shown.

curves along the v_1/v_3 diagonal [Fig. 5(b)] are particularly poor, unable to fully capture the strong anharmonicity to large negative coordinates for states S_2 and S_3 .

Compared to the earlier vibronic coupling model of Köppel *et al.*⁷ the new model not only goes to higher orders in the diabatic surfaces, but the ADC(2) electronic structure calculations used in earlier work placed the A_2 state just 0.1 eV above the lowest excited A_1 singlet state. The ADC(2) model Hamiltonian also had

quite different coupling constants that resulted in a very different spectrum.

B. Absorption spectrum

Time-dependent wavepacket calculations were performed using the ML-MCTDH method on the five-state 21-mode vibronic coupling model. Propagations were run for 200 fs starting with a

vertical excitation of the ground-state vibrational wavefunction to either the bright S_1 or S_2 state. This provides an autocorrelation function out to 400 fs. The calculated photo-absorption spectra obtained from the Fourier transform of the autocorrelation functions are shown in Fig. 6(a), both separately and summed. In Fig. 6(b), the summed spectrum is compared to the experimental spectrum of Holland *et al.*² After taking into account the zero point energy of the initial wavepacket, the calculated spectra have been shifted by -0.05 eV. The calculated vertical excitation energies are thus in excellent agreement with the experimental ones.

The model Hamiltonian clearly reproduces the features on the rising edge of the photo-absorption spectrum very well. The spacing of the progression on the rising edge agrees excellently between calculation and experiment, and the width is also in good agreement. The exponential damping function of 150 fs used to reduce edge artifacts when calculating the spectrum is equivalent to convoluting spectral lines by a Lorentzian of 9 meV, i.e., negligible in this broad spectrum. The broad featureless underlying spectrum is thus due to the vibronic coupling between states as this governs the lifetimes and hence spectral broadening. The model thus correctly accounts for this coupling. The simulation even reproduces the features at the onset of the spectrum, which have previously been assigned as hot bands, which means that they are not.⁶

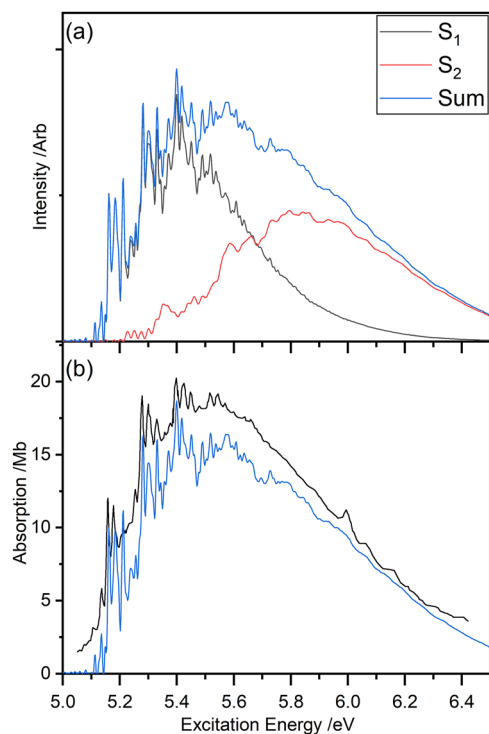


FIG. 6. (a) Calculated photo-absorption spectra for excitation from the S_0 to the S_1 and S_2 states of thiophene with all modes included in the model. (b) The experimental photo-absorption spectrum of thiophene taken from Holland *et al.* with the sum of the two calculated spectra. The calculated energies have been shifted by -0.05 eV.²

The only features missing are the structure at around 6 eV. This feature is probably due to a Rydberg state of thiophene that was not included in the *ab initio* calculations.² The S_3 state has the correct energy, but a calculation of the spectrum after excitation to the \tilde{C} state using the model Hamiltonian results in a broad band due to the strong coupling to the other states. The weak oscillator strength for this state then means that it does not appreciably change the overall spectrum shown in Fig. 6.

To confirm the quality of the fit, a 7 Hz high pass Fourier transform filter was applied to both the calculated absorption spectrum and the experimental spectrum of Holland *et al.*² Applying this filter removes the broad featureless spectral component and leaves just the structure. The results of this are shown in the [supplementary material](#), and the agreement is excellent.

Given the similarity of the calculated and measured absorption spectra, the VC Hamiltonian clearly provides a good model of the early-time dynamics of thiophene after photoexcitation, capturing the state energies around the Franck–Condon point and the frequencies of the vibrations and the couplings between them. In Secs. III C–III E, the model will be used to help assign the spectral features and understand how the couplings between the modes and states lead to the observed spectrum.

C. Assigning the spectrum

The spectrum can be assigned by running calculations including subsets of modes and couplings to see what gives rise to the features observed. Absorption spectra are usually dominated by frequencies from the totally symmetric vibrations, which in the absence of vibronic coupling are the only modes that can be excited after absorbing a photon. In Fig. 7(a), the calculated photo-absorption spectrum of thiophene is shown for excitation from the ground state into \tilde{A} using a Hamiltonian including only the eight a_1 modes and the on-diagonal κ (*intra-state*) coupling terms. This is the spectrum that would be produced by a calculation of the Franck–Condon factors for the transition. The comb shown above the spectrum represents the frequencies of the progressions on the rising edge of the spectrum. There are triplets, three peaks separated by 0.02 and 0.03 eV, which are part of progression separated by a frequency of 0.12 eV. It is clear that this spectrum does not match the experimental spectrum: the peaks are near the fundamental frequencies (shown by arrows), which bear no relationship to the progressions observed. Vibrational and vibronic couplings are thus key to modeling the photo-absorption spectrum of thiophene.

Figure 7(b) shows the changes to the Franck–Condon spectrum if the inter-state (λ) coupling terms between \tilde{X} and \tilde{A} are included along with the on-diagonal linear terms for the a_1 mode calculation. As both states have the same symmetry (A_1), these couplings are only non-zero for the a_1 vibrations and have particularly large values for $\nu_3, \nu_7, \nu_{11}, \nu_{13}$, and ν_{16} . Again, this model does not capture the full behavior of thiophene following photoexcitation. However, the vibronic coupling has had a significant effect on the spectrum. The ν_{16} peak, which is the most intense in the Franck–Condon spectrum, has reduced in intensity and split. More importantly, modes ν_{11} and ν_{13} are now degenerate and give rise to a single intense peak at the frequency of the progression of the triplets. Previous work² tentatively suggested that the progression

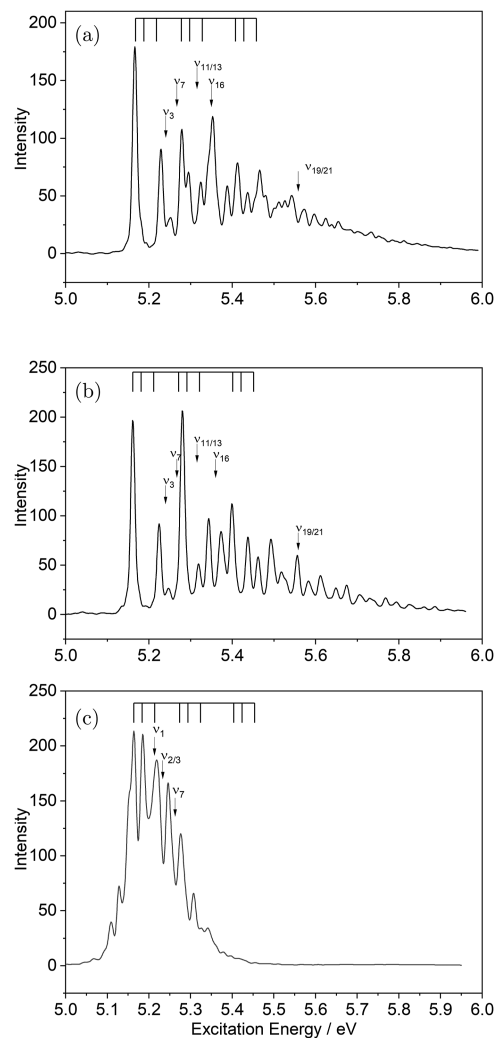


FIG. 7. Calculated photo-absorption spectrum of thiophene for excitation into the \tilde{A} state including (a) all totally symmetric modes and only on-diagonal linear (κ) terms; (b) all totally symmetric modes, but inter-state coupling terms between \tilde{X} and \tilde{A} were also included along with the on-diagonal linear terms; and (c) only modes ν_1 , ν_2 , ν_3 , and ν_7 with all relevant parameters. The combs mark where the experimental vibrational progressions are found. The arrows indicate the positions of the vibrational fundamentals. The spectra have been shifted to line up with the onset of the experimental progression.

is due to the excitation of the ν_{11} mode (ν_6 in that paper) on the grounds of symmetry. We confirm this assignment and can explain the large drop in frequency of ~ 0.015 eV (120 cm^{-1}). We also extend the assignment to note that this peak is a compound of both the ν_{11} and ν_{13} modes.

Finally, a model Hamiltonian including the four strongly coupled low frequency vibrational modes was used. These are ν_1 , ν_2 , ν_3 , and ν_7 , and the model included all couplings involving these vibrations. Modes ν_1 and ν_2 are out of plane ring vibrations, while modes ν_3 and ν_7 are in-plane bends of the C–S–C bond. These normal modes are shown in Fig. 3. In Fig. 7(c), the photo-absorption

spectrum calculated using this four-mode five-state Hamiltonian is shown. The calculation captures a key feature seen in the experimental results, namely the vibrational triplet seen throughout the spectrum. The spacings of this progression match the spacings of the previously unassigned progression on the rising edge of the experimental spectra. This calculation allows us to assign the structure as due to both inter-state and intra-state couplings between these four modes.

While these numerical experiments do not give us a detailed mechanism of the exact role played by each vibration in the spectrum, it does provide an assignment of the spectral peaks in terms of the vibrations they relate to. The triplet peaks in the spectrum are thus assigned to combinations of the strongly coupled vibrations ν_1 , ν_2 , ν_3 , and ν_7 . Both Duschinsky rotations and anharmonic terms in the Hamiltonian are needed, along with inter-state vibronic coupling. Only when all the vibrations and terms are included, does this set of spacings result and it is difficult, if not impossible, to disentangle this any further. The spacing between the triplets is due to a progression given by the ν_{11} and ν_{13} vibrations, which, as shown above, have very similar frequencies once the vibronic coupling between the \tilde{X} and \tilde{A} states is considered.

D. Diabatic population dynamics

From the wavepacket propagation, it is possible to extract the dynamics of the wavepacket motion on the diabatic thiophene surfaces. The change in diabatic state populations with time for initial excitation into the \tilde{A} state (equivalent to S_1 at the Franck–Condon point) is shown in Fig. 8(a). To check whether the population is reaching a plateau, the propagation was extended to 250 fs. The population in \tilde{A} shows a constant decay rate and does indeed reach a plateau at this time, with a population of around 0.6. Population is transferred to all four of the other states. As shown in the inset, most of the population is initially transferred into \tilde{B} and \tilde{D} . This population in \tilde{B} has largely decayed away after 20 fs, with a brief recovery in population around 70 fs. Between 20 and 70 fs, most of the transferred population is in \tilde{D} , which, after peaking around 40 fs, decays away to remain at a near constant value from about 80 fs until a small recovery around 200 fs. In contrast, the populations in \tilde{X} and \tilde{C} show a slow constant increase in population, both reaching about 0.1 by 250 fs.

State \tilde{D} clearly plays a key role in how the population moves between electronic states from the \tilde{A} state. The initial transfer into \tilde{B} occurs within 20 fs. A rise in the \tilde{D} state population is then seen, which is accompanied by a strong oscillation with a period of around 21 fs, indicating that the population is decaying from \tilde{B} by crossing to \tilde{D} . This period is equivalent to a frequency of 1570 cm^{-1} (0.19 eV). This is presumably due to the ν_{16} vibration, which leads to a low lying crossing between \tilde{A} and \tilde{B} [Fig. 4(f)]. Changes in population in \tilde{A} are also mirrored in \tilde{D} : a peak in the oscillating signal on \tilde{A} is matched by a trough in the \tilde{D} population. Furthermore, between 100 and 180 fs, the drop in the \tilde{D} population is matched by a revival in the \tilde{A} population, with a revival in \tilde{D} from 200 to 250 fs matched by another drop in \tilde{A} . This indicates there is also a direct transfer between \tilde{A} and \tilde{D} .

It is interesting to compare these theoretical results to the experimental analysis of Wu *et al.*⁸ From their resonance Raman spectroscopy, they expected an initial transfer of population from S_1 to a B_2 and an A_2 electronic state; from our calculations, \tilde{B} is a

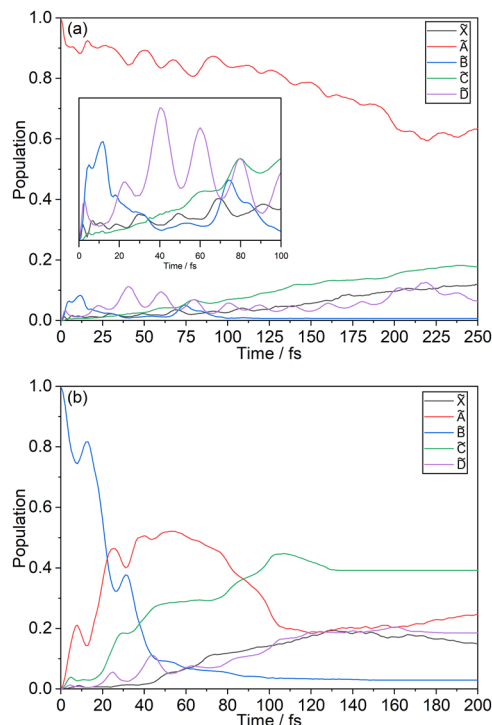


FIG. 8. Diabatic state populations of thiophene following excitation into (a) the \tilde{A} state and (b) the \tilde{B} state using the full 21 mode Hamiltonian. The inset in panel (a) shows the early time populations of the initially unpopulated electronic states.

B_2 electronic state, while \tilde{D} is an A_2 state. Therefore, the population transfer we observe agrees with these Raman results. There has been a previous ultrafast pump–probe spectroscopy measurement where S_1 is initially populated by Weinkauff *et al.*⁹ They observed an 80 fs decay, attributed to structural relaxation on the S_1 excited state surface, followed by a fast decay (25 fs) leading to ring opening; there was also a long-lived component (>50 ps).

The experimental timescales are not directly comparable with those seen in the simulation due to the temporal width of the pulses used in the experiments. The resulting narrow bandwidth (less than 0.03 eV) excites a narrow range of vibrational states rather than creating a full wavepacket as used in the simulations. However, the structural relaxation could correspond to the transfer from \tilde{A} to \tilde{B} , which stays on the S_1 state and results in ring-puckering. The ring-opening, as will be examined in more detail below, is then due to crossing to the \tilde{C} and \tilde{D} states.

The change in diabatic state populations with time after initial excitation into the \tilde{B} state (equivalent to S_2 at the Franck–Condon point) is shown in Fig. 8(b). The dynamics are very different from that in the \tilde{A} state. In this case, the population in \tilde{B} rapidly decays, with a time constant of around 20 fs, ending up with a population of just 0.05 in \tilde{B} after 100 fs. The population is transferred from \tilde{B} initially into \tilde{A} and, at later times, into \tilde{C} and \tilde{D} . At around 100 fs, the \tilde{A} population crosses into \tilde{C} , and at longer times, most of the population ($\sim 40\%$) is in \tilde{C} with the remaining population divided equally between \tilde{X} , \tilde{A} , and \tilde{D} . As with excitation into \tilde{A} , there is a

visible oscillation in the populations of the states, this time with a spacing of about 16 fs, a frequency of ~ 2100 cm^{-1} (0.26 eV). As there is no obvious vibration of this frequency able to mediate the population transfer, and this is seen directly after excitation, this must be a Rabi-like oscillation with the lower state and relates to an effective energy gap between the states.

The time-resolved experiments by Schalk *et al.*¹⁰ used a pump wavelength that would excite into the \tilde{B} state. They divided the observed dynamics into two regions. The first had two decay times of 25 and 400 fs. The second had a rise of 25 fs followed by an 80 fs decay similar to that seen in the lower energy pump experiments of Weinkauff. This 80 fs decay time they also attribute to ring-puckering, and, while they did not see the 25 fs subsequent fast decay, they saw a slow 450 fs decay which they attributed potentially to ring-opening. The first region can be clearly related to the decay of the \tilde{B} state in Fig. 8(b), which has a fast initial decay followed by a slow component. The rise at the start of the second region is the population flow into the \tilde{A} state, and the 80 fs decay is then again decay from the \tilde{A} state.

E. Structural dynamics

The one-dimensional cuts through the potential surfaces in Figs. 4 and 5 show the existence of energy minima for the various diabatic states. The energy ordering and relative positions of the minima further indicate that there are a number of possible minima on both the S_1 and S_2 adiabatic surfaces, with the one-dimensional minima being part of a minimum energy channel.

To find the actual lowest energy points on the surfaces, energy minimization calculations were run starting from geometries that were combinations of the one-dimensional minima coordinates. For the S_1 state, the following mass weighted coordinates were taken for each mode, a value of 5 for Q_1 and 2 for Q_2 . For Q_3 , there were two possible minima at 1 and -4 , and for Q_5 , there were three possible minima at 0 and ± 5 . Therefore, four starting geometries were used for the optimizations ($Q_5 = \pm 5$ are symmetrically equivalent). Two distinct minima were found. The coordinates of these minima are given in the [supplementary material](#).

One minimum has an energy of 5.23 eV. It is a ring-puckered structure close to the Franck–Condon point, but with the sulfur atom out-of-plane. The second minimum is much lower in energy at 2.77 eV. This is a ring-opened structure, with a large displacement along Q_7 . It should be noted that the structure remains planar. These minima are shown in a two-dimensional cut through the adiabatic S_1 potential in the space of Q_5 and Q_7 in Fig. 9. The two channels leading to the minima are clear, and the minimum energy structure for each channel is shown alongside.

The structures fit with the correlation of the minima to the diabatic states. The ring puckered structure with small displacements from the Franck–Condon point comes from the \tilde{A} diabatic state, which is the $\pi\pi^*$ excitation, whereas the ring-open structure with large displacements along Q_3 , Q_5 , and Q_7 correlates with the \tilde{C} diabatic state with its $\pi\sigma^*$ character.

A similar search on the S_2 adiabatic surface found four distinct minima. Among them, three, at 5.34, 5.50, and 5.68 eV, are ring puckered structures close to the Franck–Condon point, while the fourth is again a low energy (3.95 eV) structure, which is an in-plane ring-open structure similar to that in Fig. 9. It is not straightforward to associate the ring-puckered structures with particular diabatic

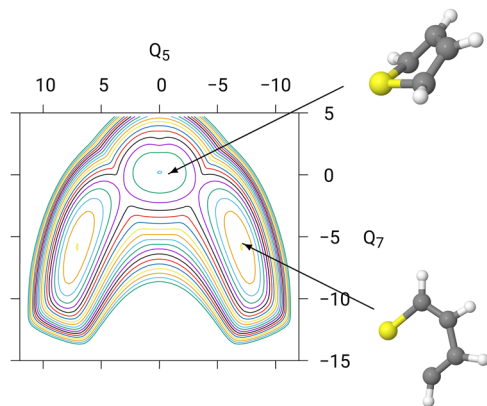


FIG. 9. Cut through the S_1 adiabatic potential surface along modes ν_5 and ν_7 . All other coordinates have a value of zero, except Q_1 , which had a value of 5.0. The structures associated with each minimum are also plotted.

states, but the ring-open structure clearly correlates with the $\tilde{D}(\pi\sigma^*)$ diabatic state.

As a result of this analysis, the transfer of diabatic state population from states \tilde{A} and \tilde{B} to \tilde{C} and \tilde{D} can be considered as moving from ring-closed to ring-opened structures. When exciting to the \tilde{A} state, it is thus expected that after 200 fs, $\sim 30\%$ of the thiophene will be in a ring-open form. If excited to the \tilde{B} state, however, $\sim 60\%$ will have ring-opened after 200 fs.

IV. DISCUSSION AND CONCLUSIONS

In conclusion, by applying a high-order vibronic coupling model and the MCTDH method to the excited state dynamics of thiophene, we have been able to assign the long unassigned vibronic features in the ultraviolet absorption spectrum of thiophene. The agreement between the calculated and measured spectra is excellent, requiring only a small shift of 0.05 eV to align the first peak. Both the spectral features and width are in near quantitative agreement, given that all parameters used in the model, including vertical excitation energies, that were taken directly from the *ab initio* calculations support the quality of the CASPT2 treatment taken from the earlier work of Schnappinger *et al.*¹²

The spectra due to the diabatic \tilde{A} and \tilde{B} states overlap strongly, with the start of the \tilde{B} band only 0.1 eV higher in energy than the \tilde{A} band even though the vertical excitation is 0.4 eV higher. The spectral features arise due to the vibrational and vibronic couplings of a number of modes in the S_0 – S_4 manifold. The four vibrations ν_1 , ν_2 , ν_3 , and ν_7 are responsible for the narrowly spaced triplet of peaks on the rising edge of the spectrum, while the combination of ν_{11} and ν_{13} provides the progression repeating this feature to higher energies. This progression has previously been assigned to the ν_6 vibration. It is also found that the initial small peaks below the first sharp peak at 5.15 eV are also due to the coupled vibrations and not due to hot bands as previously thought. This brings the origin of the band down in energy to just above 5.1 eV.

The quality of the spectrum means that the vibronic coupling model is a good description of the potential surfaces and couplings around the Franck–Condon point. It can thus also be used to gain

insights in the photo-excited dynamics of thiophene. While the \tilde{C} and \tilde{D} states are dark, they both play a role in the dynamics, and, indeed, the features of the spectrum require the inclusion of these states in the model. The importance of these states is also seen in a recent study of the 1 + 1 REMPI spectra.³⁴ The measured photoelectron angular distributions (PADs) indicate that after photoexcitation to this band, electrons are emitted from orbitals with the σ character, which indicates that crossing occurs to these two states from the initially populated \tilde{A} and \tilde{B} .

The bright excited-states have a very different population dynamics. If excited into the lower, \tilde{A} , state, the initial population is found to relax fairly slowly, decreasing by $\sim 40\%$ over 200 fs, and driven initially by the ν_{16} vibration. This final population is spread fairly evenly over the ground state and \tilde{C} and \tilde{D} . In contrast, excitation to the \tilde{B} state results in fast relaxation to \tilde{A} followed by further crossing to \tilde{X} , \tilde{C} , and \tilde{D} . The initially populated state is depleted after 100 fs. This very different behavior explains the different dynamics seen by Weinkauff *et al.*⁹ and Schalk *et al.*,¹⁰ who excited into the \tilde{A} and \tilde{B} bands, respectively.

One of the largest controversies in the photochemistry of thiophene is whether, following photoexcitation, it ring opens or instead puckers out of plane. There is no clear experimental evidence for either, although the resonance Raman study by Wu *et al.* expected ring opening to occur due to the importance of the observed anti-symmetric C–S–C stretch.⁸ From the analysis of the state population dynamics and structures related to the minima on the potential surfaces, the simulations clearly show that both are likely to happen. The ring puckering is due to the vibronic activation of the out-of-plane ν_1 and ν_2 modes after excitation to the \tilde{A} state. In contrast, in-plane ring opening happens due to vibronic activation of the anti-symmetric C–S–C vibration ν_5 which leads to crossing from \tilde{A} to \tilde{B} and on to the ring open states \tilde{C} and \tilde{D} . Exact timescales or yields for each will be difficult to extract due to the strong coupling of all the modes and states involved, but the ring-opening is expected to occur on a 100 fs timescale and increase in importance with excitation energy as crossing to the higher states becomes easier.

The second controversy in the photochemistry of thiophene is whether triplet states are involved or not. The question arises due to the presence of the sulfur atom suggesting a relatively large spin–orbit coupling and the importance of triplet states in the photochemistry of bithiophenes (and larger conjugated systems). Although thiophene has been found to demonstrate a very weak phosphorescence, it is unclear how important triplets are to the dynamics following photoexcitation.³⁵ As we did not include spin–orbit coupling, the work presented here is not able to answer this question. Certainly, our calculations show that triplet electronic states are not required to explain thiophene's absorption spectrum and, due to the strong vibronic coupling, are unlikely to play a significant role in the excited state dynamics of the first few 100 fs. Schnappinger *et al.* used surface hopping calculations to look at the interplay between intersystem crossing and internal conversion and came to conclusion that the triplet states were important in controlling how long it took for thiophene to move from the ring open form back into the closed form.¹² However, like the majority of previous theoretical studies on thiophene, the \tilde{D} state was not included in this work. As we have demonstrated, this state plays a significant role in the early dynamics after photoexcitation.

Therefore, to confirm the involvement of triplet states, it will be necessary to repeat these calculations, including this 1A_2 state and the triplet states.

In conclusion, the work presented here provides an assignment and coherent explanation for the structures seen in the “simple” UV absorption spectrum of thiophene. This work thus provides a platform for further understanding of this molecule by elucidating the main ingredients required to describe the excited-state dynamics of this molecule. The absorption of a photon by thiophene in this energy region is seen to lead to a complicated dynamics involving four strongly coupled electronic states and eight vibronically and vibrationally coupled modes. A fast population transfer (<100 fs) between the states is seen along with both ring puckering and ring opening. Future work will be needed to look at the question such as the involvement of triplet states and the long-time dynamics, but that is beyond the capabilities of the vibronic coupling model used here.

SUPPLEMENTARY MATERIAL

The [supplementary material](#) encompasses the coordinates of the optimized ground state structure, pictures of the vibrational normal modes, cuts through the vibronic coupling model potentials, and the wavefunction tree and basis sets used in the ML-MCTDH calculations. Details are also given of datasets containing the files from the simulations presented. These are available from the UCL Data Repository (<https://https://rdr.ucl.ac.uk/>) at <http://doi.org/10.5522/04/26076520>.

ACKNOWLEDGMENTS

This work was funded, in part, by the EPSRC program under Grant No. EP/V026690/1.

AUTHOR DECLARATIONS

Conflict of Interest

The authors have no conflicts to disclose.

Author Contributions

Michael A. Parkes: Conceptualization (equal); Formal analysis (equal); Investigation (equal); Validation (lead); Visualization (lead); Writing – original draft (equal); Writing – review & editing (equal). **Graham A. Worth:** Conceptualization (equal); Data curation (equal); Funding acquisition (lead); Investigation (equal); Methodology (lead); Writing – original draft (equal); Writing – review & editing (equal).

DATA AVAILABILITY

The data that support the findings of this study are available within the article and its [supplementary material](#).

REFERENCES

- ¹C. Kok, C. Doyranlı, B. Canimkurbey, S. Pıravadılı Mucur, and S. Koyuncu, *RSC Adv.* **10**, 18639 (2020).
- ²D. M. P. Holland, A. B. Trofimov, E. A. Seddon, E. V. Gromov, T. Korona, N. de Oliveira, L. E. Archer, D. Joyeux, and L. Nahon, *Phys. Chem. Chem. Phys.* **16**, 21629 (2014).

- ³D. B. Jones, M. Mendes, P. Limão-Vieira, F. Ferreira Da Silva, N. C. Jones, S. V. Hoffmann, and M. J. Brunger, *J. Chem. Phys.* **150**, 064303 (2019).
- ⁴A. Prlj, B. F. Curchod, and C. Corminboeuf, *Phys. Chem. Chem. Phys.* **17**, 14719 (2015).
- ⁵A. Prlj, B. F. Curchod, A. Fabrizio, L. Floryan, and C. Corminboeuf, *J. Phys. Chem. Lett.* **6**, 13 (2015).
- ⁶E. J. Beiting, K. J. Zeringue, and R. E. Stickel, *Spectrochim. Acta, Part A* **41**, 1413 (1985).
- ⁷H. Köppel, E. V. Gromov, and A. B. Trofimov, *Chem. Phys.* **304**, 35 (2004).
- ⁸X.-F. Wu, X. Zheng, H.-G. Wang, Y.-Y. Zhao, X. Guan, D. L. Phillips, X. Chen, and W. Fang, *J. Chem. Phys.* **133**, 134507 (2010).
- ⁹R. Weinkauff, L. Lehr, E. W. Schlag, S. Salzmann, and C. M. Marian, *Phys. Chem. Chem. Phys.* **10**, 393 (2008).
- ¹⁰O. Schalk, M. A. Larsen, A. B. Skov, M. B. Liisberg, T. Geng, T. I. Sølling, and R. D. Thomas, *J. Phys. Chem. A* **122**, 8809 (2018).
- ¹¹G. Cui and W. Fang, *J. Phys. Chem. A* **115**, 11544 (2011).
- ¹²T. Schnappinger, P. Kölle, M. Marazzi, A. Monari, L. González, and R. de Vivie-Riedle, *Phys. Chem. Chem. Phys.* **19**, 25662 (2017).
- ¹³M. Stenrup, *Chem. Phys.* **397**, 18 (2012).
- ¹⁴S. Salzmann, M. Kleinschmidt, J. Tatchen, R. Weinkauff, and C. M. Marian, *Phys. Chem. Chem. Phys.* **10**, 380 (2008).
- ¹⁵P. Kölle, T. Schnappinger, and R. de Vivie-Riedle, *Phys. Chem. Chem. Phys.* **18**, 7903 (2016).
- ¹⁶A. Viel and W. Eisfeld, *J. Chem. Phys.* **120**, 4603 (2004).
- ¹⁷L. Bosse, B. P. Mant, D. Schleier, M. Gerlach, I. Fischer, A. Krueger, P. Hemberger, and G. Worth, *J. Phys. Chem. Lett.* **12**, 6901 (2021).
- ¹⁸V. J. Rani, A. K. Kanakati, and S. Mahapatra, *J. Phys. Chem. A* **126**, 6581 (2022).
- ¹⁹H.-J. Werner, P. J. Knowles, G. Knizia, F. R. Manby, M. Schütz, P. Celani, W. Györfy, D. Kats, T. Korona, R. Lindh, A. Mitrushenkov, G. Rauhut, K. R. Shamasundar, T. B. Adler, R. D. Amos, A. Bernhardsson, A. Berning, D. L. Cooper, M. J. O. Deegan, A. J. Dobbyn, F. Eckert, E. Goll, C. Hampel, A. Hesselmann, G. Hetzer, T. Hrenar, G. Jansen, C. Köppl, Y. Liu, A. W. Lloyd, R. A. Mata, A. J. May, S. J. McNicholas, W. Meyer, M. E. Mura, A. Nicklass, D. P. O’Neill, P. Palmieri, D. Peng, K. Pflüger, R. Pitzer, M. Reiher, T. Shiozaki, H. Stoll, A. J. Stone, R. Tarroni, T. Thorsteinsson, and M. Wang, *MOLPRO, version 2015.1, a package of ab initio programs*, 2015.
- ²⁰C. Cattarius, A. Markmann, and G. A. Worth, The VCHAM program, see <http://www.pci.uni-heidelberg.de/tc/usr/mctdh/>, 2007.
- ²¹G. A. Worth, K. Giri, G. W. Richings, I. Burghardt, M. H. Beck, A. Jäckle, and H.-D. Meyer, The QUANTICS package, version 1.1, 2015.
- ²²G. A. Worth, *Comput. Phys. Commun.* **248**, 107040 (2020).
- ²³H.-D. Meyer, U. Manthe, and L. S. Cederbaum, *Chem. Phys. Lett.* **165**, 73 (1990).
- ²⁴M. Beck, A. Jäckle, G. Worth, and H.-D. Meyer, *Phys. Rep.* **324**, 1 (2000).
- ²⁵G. A. Worth, H.-D. Meyer, H. Köppel, L. S. Cederbaum, and I. Burghardt, *Int. Rev. Phys. Chem.* **27**, 569 (2008).
- ²⁶*Multidimensional Quantum Dynamics*, edited by H.-D. Meyer, F. Gatti, and G. A. Worth (John Wiley & Sons, Ltd., 2009).
- ²⁷A. Lehr, S. Gómez, M. A. Parkes, and G. A. Worth, *Phys. Chem. Chem. Phys.* **22**, 25272 (2020).
- ²⁸H. Wang and M. Thoss, *J. Chem. Phys.* **119**, 1289 (2003).
- ²⁹U. Manthe, *J. Chem. Phys.* **128**, 164116 (2008).
- ³⁰O. Vendrell and H.-D. Meyer, *J. Chem. Phys.* **134**, 44135 (2011).
- ³¹D. Mendive-Tapia, T. Firmino, H.-D. Meyer, and F. Gatti, *Chem. Phys.* **482**, 113 (2017).
- ³²*NIST Chemistry WebBook: NIST Standard Reference Database Number 69*, edited by P. J. Linstrom and W. G. Mallard (National Institute of Standards and Technology, Gaithersburg, MD, 2021).
- ³³D. Opalka and W. Domcke, *J. Chem. Phys.* **132**, 154108 (2010).
- ³⁴J. J. Broughton, S. Patra, M. Parkes, G. A. Worth, and H. H. Fielding, “A multiphoton ionisation photoelectron imaging study of thiophene,” *Phys. Chem. Chem. Phys.* (2024) (submitted).
- ³⁵R. S. Becker, J. Seixas de Melo, A. L. Maçanita, and F. Elisei, *J. Phys. Chem.* **100**, 18683 (1996).